Waste glass as a source for green synthesis of microporous adsorbent for efficient removal of heavy metals

Jean-Baptiste Mawulé Dassekpo[a,*], Haiying Zhong[b], Chonkei Iong[c], Zhijun Dong[a], Ningning Shao[a], Innocent Sègla Dassekpo[d], Dongmin Wang[e], Jianqiao Ye[f]

[a] Institute of Technology for Marine Civil Engineering, Shenzhen Institute of Information Technology, 518172, PR. China
[b] Institute of Traffic and Environment, Shenzhen Institute of Information Technology, 518172, PR. China
[c] Department of Civil and Environmental Engineering, Harbin Institute of Technology (Shenzhen), 518055, China
[d] Genetics, Biotechnology & Seed Science (GBioS), FSA, University of Abomey-Calavi, 01 PO Box 526, Republic of Benin
[e] School of Chemical and Environmental Engineering, China University of Mining and Technology-Beijing, 100083, China
[f] School of Engineering, Lancaster University, Lancaster LA1 4YR, UK

*Corresponding author email: dassekpo.jb@sziit.edu.cn

Abstract

Microporous analcime Adsorbent (MaA) was cogently synthesized in a hydrothermal reaction where a waste silica glass powder was mixed into NaOH solution. The satisfactory reaction properties were achieved by regulating the conditioning time (*Ct*), reaction temperature (*Rt*), and relative ratio of the reactants (*Rr*= SiO_2:Na_2O). XRF, XRD, SEM, BET, FTIR, AFM, TG and TEM analysis formed part of the selected samples. The prepared MaA adsorbent was then applied to treat Pb^{2+}, Cd^{2+} and Cu^{2+} ions, thus effectively allowing the physicochemical properties (pH, temperature and contact duration), on the adsorption amount to be examined. Upon completion, the results indicated that the initial pH as well as the contact duration had notable effect on the adsorption amount. Conversely, the temperature change had an insignificant effect on the equilibrium adsorption amount. In addition, a dosage of 0.1 g/L of MaA, concentration of 100 mg/L, pH ranging from 6~8, and temperature of about 25°C were found to be the optimum process conditions for the adsorption of the examined heavy metal samples, whereas difference in contact time was recorded as follows: 1h for Pb^{2+} and Cu^{2+} ions

with adsorption amounts of 150.26 mg/g and 148.19 mg/g, respectively; and 3 h for Cd^{2+} ion with adsorption equal to 145.22 mg/g. In the analysis of the trend, the coefficients of correlation (R^2=0.99) of the Langmuir isotherm model were increasingly consistent compared to Freundlich isotherm model (R^2 from 0.10 to 0.55), thus indicating that the process to be a homogeneous monomolecular layer adsorption. Moreover, the kinetic aspects were similarly consistent in relation to quasi-secondary kinetic equation, which then further established that the process was primarily controlled by ion exchange, extra-particle, intra-particle, and liquid film diffusion.

Keywords: Waste Glass; Green Synthesis; Analcime Zeolite; Heavy metals; Adsorption kinetics; Wastewater treatment.

1. Introduction

The adverse impact of solid waste pollution and other harmful substances on the natural ecosystem, human well-being, and the overall life's quality is a grave and critical global predicament. Human activities that release contaminated pollutants into the air, water and soil have continuously worsened the environment. Accordingly, whereas the management of such pollutants remains a great challenge, it is essential that it is resolved with utmost urgency. An effective and efficient implementation of management practices such as recycling, reusing and rational disposal could minimize pollution risks thereby optimizing the safety and protection of the environment. It has been estimated that the annual worldwide production of solid waste is about 2.01 billion tons, with 4−8% of the total volume comprising glass waste [1, 2]. As a solid material with unique vitreous properties and stable silicate composition, glass is commonly used in various applications. For instance, in early 2021, approximately 22.75 million tons of waste glass was recorded in China, of which about 10.05 million tons were recycled, corresponding to a 44.2% recycling rate [3]. Although glass can be converted from

the solid broken or non-broken waste to produce by melting at high temperature a new glass product repeatedly without losing its quality, its sorting by color and from other waste remain a big challenge and onerous, especially in China where they are a lack of waste sorting infrastructures. Sorting the glass from multitudes of waste materials or by color increases undeniably its market value. Furthermore, because of its heavy weight, transportation of glass wastes to recycling plants demands a comparatively higher logistical cost. Thus, from an economic, environmental and health perspective, recycling and re-utilization of waste glass is a necessity.

As a non-biodegradable material by nature, glass has a very long-life cycle, and so as a waste, adversely impacts the environment for an extended period without altering its chemical properties. In fact, perpetual recycling of glass hardly alters its physicochemical properties due to the stable silicate (SiO_2) and alumina (Al_2O_3) content. The two compounds are nearly similar to zeolite in composition, thus creating the likelihood of a synthesis of functional minerals through a suitable hydrothermal reaction for its applications as adsorbents. This property, however, makes it a filter composite to remove harmful constituents [4], such as pollutants treatment from wastewater, oils and organic [5], pathogenic bacteria [6], and odors [7, 8]. In fact, over the past decades, the need for adsorbents, which can effectively eliminate the hazardous constituents from contaminated water, has increased. In particular, the need exacerbated due to the demand for clean water following pressures of population increase and industrial activities for domestic and commercial use, respectively. Likewise, growing demand for services, particularly in food production, has aggravated the degradation and pollution of natural water sources, which further worsens the state of drinking water [9-11]. Inorganic pollutants, metalloids, organic pollutants, and microorganisms pollutes water sources and are classified as heavy metals [12, 13]. Due to their large and increasing industrial use, heavy metals (HM) like lead (Pb), cadmium (Cd) and copper (Cu), etc. are of serious concern when

discharged as wastewater [14, 15] As toxins and pollutants, these elements through adsorption, bio-availability, bio-concentration, and bio-magnification exposes human physiology to reproductive, neurological, hematopoietic, skeletal, neurological, cardiovascular and renal systems disruptions [16-18]. Following these hazardous attributes, it is imperative that an alternative composite that can better absorb or eliminate heavy metals be developed.

Various methods for the elimination of HM ions from wastewater are currently available, which include the processes such as coagulation [19, 20], chemical precipitation [1, 21], ion exchange process [22, 23], membrane filtration or separation [24], reverse osmosis [25, 26] and adsorption [27-29]. Of these processes, adsorption is comparatively becoming a better alternative because of its lower cost, easier and faster operation, and wider range of applicability [30-32]. Meanwhile, the search for a suitable and promising adsorbent with high adsorption capacity, rapid adsorption, and desorption kinetics as well as low energy is very crucial to meet pilot and industrial level requirements. Consistent with the foregoing criteria, additional considerations such as long-term durability, cheaper costs, sustainability, and environmental friendliness should be prioritized. Number of suitable adsorbents for removing HM, in particular carbon nanotubes, activated carbon, graphene oxide, mesoporous silica, mesoporous carbon, clays, zeolites, metal organic frameworks and adsorbents obtained from agricultural or industrial wastes have been developed [9]. Among these adsorbents, synthetized zeolites have drawn particular attention due to that its worldwide availability, which can be found in different structures, its stable chemical compositions, good adsorption properties, simple production method, and its high affinity for heavy metals removal. Analcime ($NaAlSi_2O_6H_2O$) is a specie of zeolite and an important chemical mineral composed of 3D rigid structure, which has been utilized in recent years for diverse applications. However, pure and premium-quality analcime (ANA) is extremely rare, thus non-artificial and precious crystal must be sourced and purified to meet the industrial expectations and standard [33, 34].

Previous studies have proved that favorable analcime may be synthesized by low-cost and unhindered methods, e.g., the hydrothermal method [35, 36], especially from raw materials such as coal fly ash, rice husk, quartz syenite, pyrophyllite, and amber container glass [37-41]. Although the use of recycled glass in the synthesis of zeolites has already been documented in the literature, further studies and research are required on the hydrothermal conversion of silica glass powder into synthetized zeolite for efficient removal of heavy metals from wastewater. This work closely examines and considers the issue of hydrothermal conversion of silica glass powder into microporous adsorbent capable of treating Pb, Cd and Cu ions from wastewater. The adsorbent is produced through a clean method, featuring XRF, XRD, SEM, BET, FTIR, AFM, TG and TEM. The data provided references for facile treatment of heavy metals that may constitute a threat to human health.

2. Experimental section

2.1 Materials

Beverage soda lime glass bottles having 69.43% SiO_2, 15.35% Na_2O, and 9.27% CaO composition were used as raw material. The broken bottles were collected from Longgang District Recycling Plant (Shenzhen). To avoid any inconsistencies due to mis-coloration, only green color bottles were selected. The glasses were washed, dried, crushed to finer grit pieces, and grounded using disc ball mill with 180 rpm speed for 30 min. The obtained fine glass powder (GP) was then screened and particle size <5 μm of the powder was collected. A fixed ratio of glass powder GP:NaOH(aq, 3M) solution equal to 2:15 was adopted. The chemical compositions in percentage of the NaOH, as specified by the manufacturer are Sulfate (SO_4): 0.005, Phosphate (PO_4): 0.001, Aluminum (Al): 0.002, Calcium (Ca): 0.01, Chloride (Cl): 0.005, Nitrogen (N): 0.001, Silicate (SiO_3): 0.01, Potassium (K): 0.05, Iron (Fe): 0.001 and Heavy metals (calculated as Pb): 0.003.

2.2 Formation of the microporous analcime zeolite

The solid waste glass was converted into microporous powder through a hydrothermal reactor. The measured glass powder was added to NaOH solution and mixed for about 5 min. The mixed slurry was then poured into a hydrothermal synthesis reactor, and imperviously sealed for 3 hours at a conditioning temperature of 150°C. After the conditioning and normal cooling, the resultant mixture was filtered through vacuum filtration equipment and thereafter continuously cleaned with de-ionized water to neutralize. Finally, the resultant solid product was subjected to an 80°C drying heat for 24 hours. Fig. 1 illustrates the formation procedures of the microporous analcime (MaA).

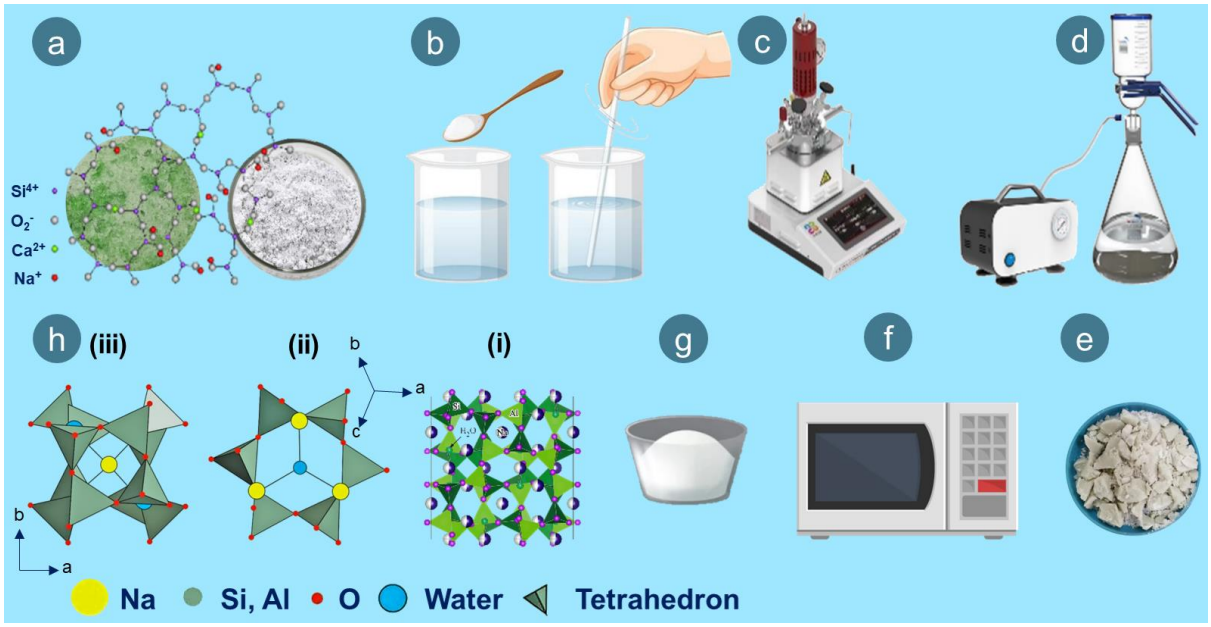

Fig. 1 Experiment illustration: (a) Silica glass powder (GP) having 69.43% SiO_2, 15.35% Na_2O, 9.27% CaO composition, (b) Pre-mixing of GP into NaOH solution, (c) Hydrothermal synthesis, (d) Filtration and de-ionization, (e) Wet analcime zeolite, (f) Drying process, (g) Microporous Analcime Adsorbent (MaA), Structure of analcime [$Na_8Al_8Si_{16}O_{48}(H_2O)_8$]: (i) Crystal structure of analcime, (ii) 6-membered rings in analcime crystal, 4-membered rings in analcime crystal.

2.3 Adsorption of HM from contaminated solutions by MaA

Adsorption kinetic of the MaA in relation to heavy metals was recorded. 0.1 grams of dried MaA was added into 10 mL solution of heavy metals with a mass fraction of 100 mg/L. The

modification of the pH's solutions was performed from 4.0−8.0. The mixtures were separately stirred at 300 r/min at temperature varying between 20-40°C. An aliquot of 2 mL of the prepared solution was withdrawn and filtrated via a syringe fitted with 0.22 μm membrane at time frames between 0−1440 min, followed by the pH control for different solution. Thereafter, the dissolution rate of Pb^{2+} Cd^{2+} and Cu^{2+} was analyzed using inductively coupled plasma mass spectrometer (Thermo Scientific iCAP RQ ICP-MS). Finally, the adsorption efficiency *(AR)* and adsorption capacity *(AC)* of the MaA composite on the heavy metal's ions were calculated using Eqs. (1-2).

$$AR\ (\%) = \frac{C_0 - C}{C_0} \times 100\% \quad (1)$$

$$AC\ (mg/g) = \frac{(C_0 - C)V}{m} \quad (2)$$

where *Co* denotes the metal ions concentration before adsorption (mg/L); *C* is the metal ions concentration after adsorption (mg/L); *V* is the volume of the aqueous solution (mL) and *m* is the mass of MaA adsorbent (g).

2.4 Characterization methods

The element composition of GP and MaA were recorded by X-ray fluorescence (XRF, Thermo Fisher ARL Perform'X). Diffraction pattern was recorded via X-ray diffractometer (XRD, D8 Advance). The structure morphology was studied using field emission scanning electron (Zeiss Gemini SEM 300), and the main chemical components distributions were collected with the aid of energy dispersive X-ray spectroscopy (X-Max^N Oxford Instruments). The total BET surface area (S_{BET}) and the distribution of the pore size were measured by Micromeritics ASAP 2460. Fourier transform infrared spectroscopy (FTIR) was used to collect the spectra at wavenumber ranging from 400−4000 cm^{-1}. AFM investigation was carried out on an Atomic Force Microscope (Dimension Icon). Thermogravimetric (TG) measurement was performed on a Differential Scanning Calorimetry (TG-DSC STA 449 F5 Jupiter). TEM

imaging was obtained on an electron microscope (Talos F200X S/TEM) equipped with a field emission gun.

3. Results and discussion

3.1 Synthesis and adsorption mechanism

Waste glass (WG) has silicate properties ($MxO\text{-}nSiO_2$ > 80%, M=Na, Ca, K, etc., x=1 or 2) and amorphous properties (~100%). The preparation of zeolite from WG is considered as an optimization of solid waste recycling. By mechanically milling WG, ultra-fine glass powder can be obtained, thereby increasing the specific surface area which consequently ensures an activating effect on the glass micro-spheres. Under an alkaline environment, the amorphous silica chains in the broken glass powder are feasible chemically. By increasing the reaction temperature, the kinetics reaction accelerates, which in turn speeds up the production of analcime zeolite crystals from the glass powder. Using waste glass as the silica source and reacting with NaOH solution in the reaction system, the main components in the waste glass, such as SiO_2, Al_2O_3, Na_2O, CaO, etc., are gradually dissolved. In general, the reactivity of glass powder in the alkali solution mainly comes from the Si dissolved in the glass body network structure. SiO_4 tetrahedron is the basic unit of the silicate glass network structure. SiO_4 tetrahedron is connected by bridging oxygen (Bridging Oxygen, BO); alkali metals such as Na, K, Ca and non-bridging oxygen (Non-Bridging Oxygen, NBO) and SiO_4 tetrahedron connection [42].

Under the hydrothermal condition, SiO_2, Al_2O_3 ions in the solution gradually crystallize and precipitate to form analcime zeolite crystals. Water molecules play an important role in the reaction as solvent and crystal grow This kind of zeolite has good adsorption, ion exchange properties and can be used as catalyzer. Hence, it interacts with heavy metal ions in the solution through ion exchange, chemical adsorption, and surface complexation (Fig. 2). Ion exchange

leads to the replacement of cations Na^+, K^+, etc. in the zeolite crystals by heavy metal ions, forming ions adsorbed on the surface or in the pores of the analcime. Oxygen atoms on the surface of zeolite are electron-rich, and chemisorption enhances the stability of adsorption through the configuration of chemical bonds within oxygen atoms on the surface of zeolite and heavy metal ions. Surface complexation further enhances the adsorption performance through the composition of complexes amidst the hydroxyl groups (OH^-) on the exterior of the analcime and the heavy metal ions.

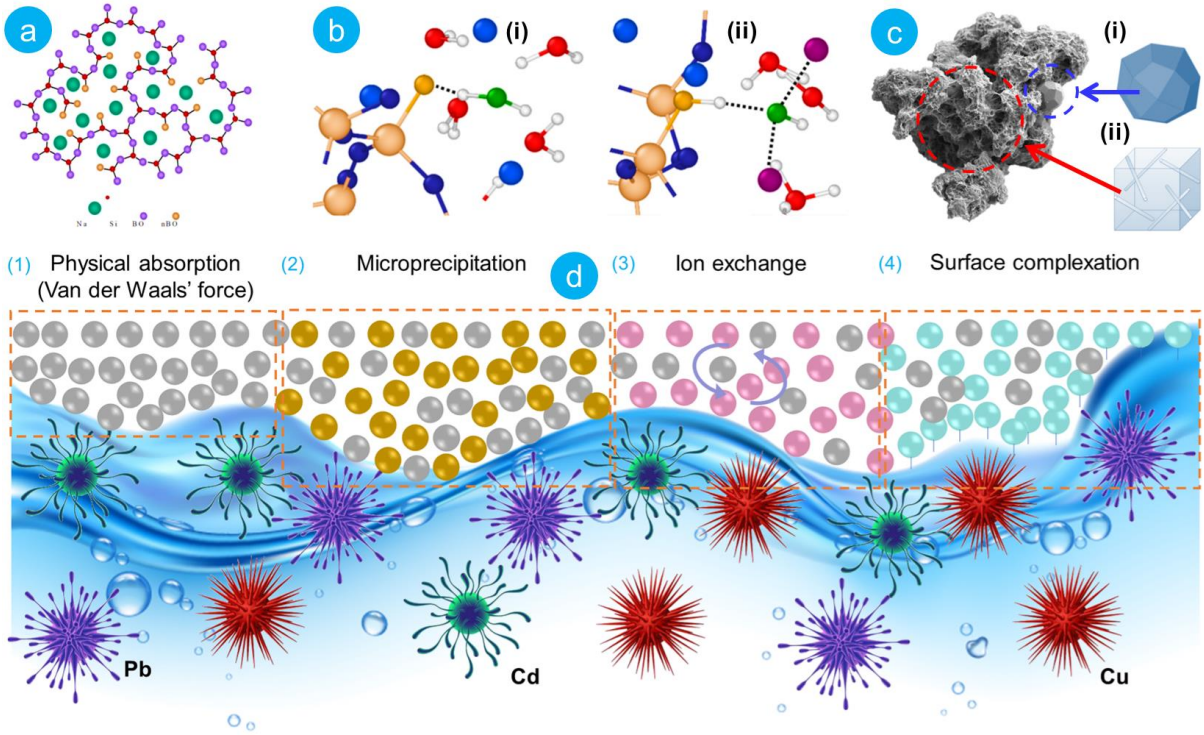

Fig. 2 Synthesis of MaA and it adsorption mechanism on heavy metals: (a) Structure of silica glass, (b) Non-bridging oxygen (NBO) atoms sites hydroxylation by water dissociation and Na−OH formation: (i) Water adsorption at the NBO site, (ii) NBO protonation (SiOH), and subsequent establishment of Na−OH interaction, (c) MaA microporous adsorbent: (i) Tetragonal trioctahedral crystalline form observed via Scanning Electron Microscope, (ii) Schematic of the pore structure, (d) Heavy metals adsorption process: (1) Physical adsorption (Electrostatic attraction−Van der Waals' force), (2) Microprecipitation, (3) Ion exchange, (4) Surface complexation.

3.2 Characterization of the microporous analcime zeolite

3.2.1 Elemental composition and morphology

The elemental composition of the glass microspheres used in the hydrothermal process were SiO_2 (69.43 wt %), Na_2O (15.35 wt %) and CaO (9.27 wt %). Other elements such as Al_2O_3, SO_3, Fe_2O_3, TiO_2, MnO, MgO and K_2O were also found in negligible percentages. Different types of glasses were distinguished according to their composition and silica mineral content varying from 65 to 75%. SiO_2 and Al_2O_3 were the main minerals in the zeolization process. During the 3 h hydrothermal treatment, the glass minerals were converted into purer analcime zeolite ($NaAlSi_2O6•H_2O$) having clearer crystallinity, as confirmed by the XRD pattern (Fig 3.a). The result is consistent with similar experiments conducted by Azizi et al. [36], affirming that well-crystallized analcime gradually formed as the synthesis time extended. In addition, the diffraction peaks of the analcime were predominant, indicating that these hydrothermal conditions are sufficient to generate pure analcime.

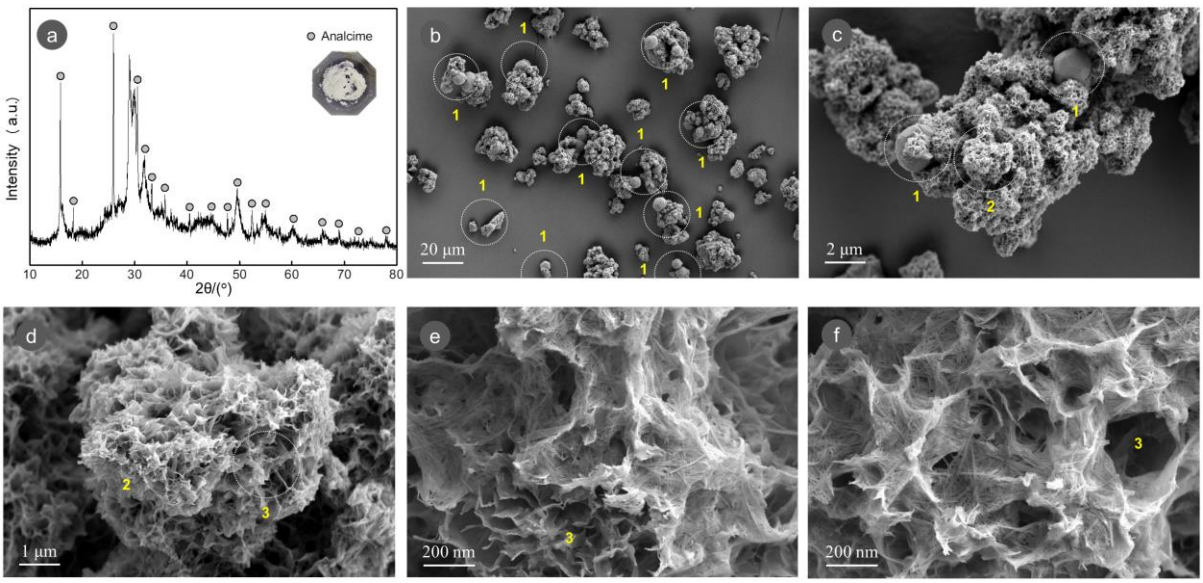

Fig. 3 XRD and SEM morphology: (a) XRD pattern showing $NaAlSi_2O6•H_2O$ as the predominant phase, (b) 20μm structure of MaA composed of many well-formed crystals, (c) 2μm structure of MaA showing two big crystals, (d) 1μm pores structure of MaA, (e, f) 200nm large-scale of the pores structure presented in MaA.

Fig 3. (b, c, d, f) are the SEM micrographs of the microporous material recorded at different magnitudes. Evidently, multiple single analcime crystals are formed on the surface or agglomerated amongst the powdery particles (Fig 3.b, c). As is widely known and generally accepted, the zeolite nucleation is often determined by various factors, including supersaturation degree of nucleation revulsion and reaction solution. The large-scale single crystals observed in the structure can be adduced to the moderate degree of nucleation, since it was revealed that until the crystals grow to the largest sizes, the small amount of nucleation can effectively supply sufficient reactive species in the reaction system [43, 44]. The micrograph in Fig 3.d shows thin lamellas agglomerated micro pores distributed over the entire surface, which are more visible at 200 nm magnitude (Fig 3.e, f). At this scale, the porosity of the material is more perceptible, and the interconnected oval-shaped pores are visible. The permeability of the structure can be attested to the fact that the glass micro spheres become soft and soluble during the hydrothermal reaction in NaOH dissolution. At this stage of decomposition, the particles lose weight, and the pressure induces vaporized gas, which generates pores in the structure of the formed crystals.

3.2.2 BET permeability and surface area

The BET permeability and the surface area (SA) of the MaA were noted, as shown in Fig 4. Specifically, the SA of MaA was recorded and was found to be around 63.69 $m^2\ g^{-1}$, with Langmuir surface area of about 70.24 $m^2\ g^{-1}$. A desorption hysteresis was observed from P/Po = 0.7 to 1.0 (Fig. 4a) due to the capillary condensation in the micro/meso-pores of MaA. Fig 4.b presents the isotherm pressure composition of MaA. The absolute pressure varied between 0-700 mmHg, and the weight N_2% ranged from 0-25. The BJH adsorption and desorption aggregate volume of pores ranging 1.0-300 nm diameter were recorded to be respectively around 0.337 $cm^3\ g^{-1}$ and 0.344 $cm^3\ g^{-1}$. Similarly, DH adsorption and desorption aggregate volume of pores from 1.7 to 300 nm in diameter are ranged from 0.338 $cm^3\ g^{-1}$ to 0.340 $cm^3\ g^{-}$

[1] (Fig. 4 c, e, g). The BJH and DH cumulative surface pore area were also recorded and presented in Fig. (4 d, f, h). It can be clearly noted that, between 1.0-300 nm, the cumulative surface area is around 52.61m² g^{-1} and 55.76 m² g^{-1}, respectively for BJH adsorption and desorption; while at 1.7-300 nm, the DH revolves around 42.91 m² g^{-1} and 47.18 m² g^{-1}, respectively, for adsorption and desorption cumulative surface area. In addition, the average diameter of adsorption and desorption pores were, respectively, 22.04 and 15.74 nm, which indicated that the porosity of MaA is higher.

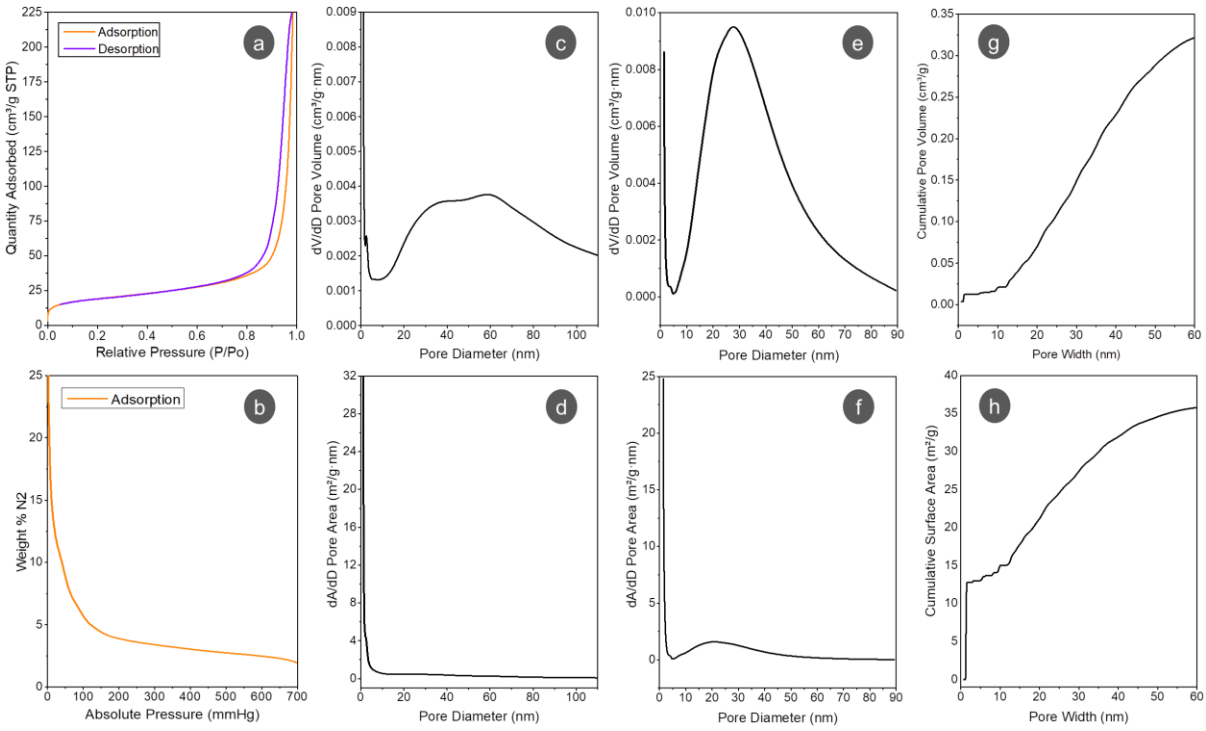

Fig. 4 BET Adsorption/Desorption isotherm results: (a) Isotherm linear plot, (b) Isotherm pressure composition, (c) BJH Adsorption dV/dD pore volume, (d) BJH Adsorption dA/dD pore area, (e) BJH Desorption dV/dD pore volume, (f) BJH Desorption dA/dD pore area, (g) Cumulative pore volume vs. Pore width, (h) Cumulative surface area vs. Pore width.

3.2.3 FTIR and AFM analysis

The morphology of MaA was further characterized by FTIR and AFM (Fig. 5). Fig. 5a shows the FTIR spectra of MaA, where the wavenumber varies from 914.12 cm^{-1} to 3400.26 cm^{-1}. The transmission percentages of 55.37, 52.92, 72.00, 92.33, 78.60, 92.42 and 91.05 were assigned respectively for 914.12, 954.19, 1040.85, 1170.38, 1420.11, 1642.82 and 3400.26 cm^{-}

[1] wavenumbers. The sharp bands at 914.12, 954.19 cm^{-1} and the shoulder bands from 1040.85 and 1170.38 cm^{-1} are due to the symmetric and asymmetric Si−O stretching oscillations. The recordings of the band at 1420.11 cm^{-1} is assigned to the vibration of CO_3^{2-} [45], and the band around 1642.82 cm^{-1} is attributed to the bending vibration of H−O−H of the adsorbed H_2O and H_2O in the interlayer. Additionally, the large-band closely at 3400.26 cm^{-1} wavenumber is due to the stretching vibration of O−H [46, 47]. Fig. 5b details the results obtained from the atomic force microscopy (AFM). The morphology of MaA shows irregular shapes with different particles sizes (Fig. 5b-i-ii), indicating the presence of multiple analcime crystals as described by the SEM results. Evaluation of the 2D Planar and 3D surfaces between -1.3~2.0 nm in Fig. 5b(i-ii) shows the thin and polished appearance of MaA. From the height-length contour through the solid line (Fig. 5b-iii), the average thickness of the porous MaA is estimated at around 0.918 nm, indicating the slenderness of MaA. Notably, the result was obtained on the surface layer of analcime without any ultrasonication treatment, which is known to significantly direct the particle size dispersion as well as enhance the constancy and steadiness of emulsions.

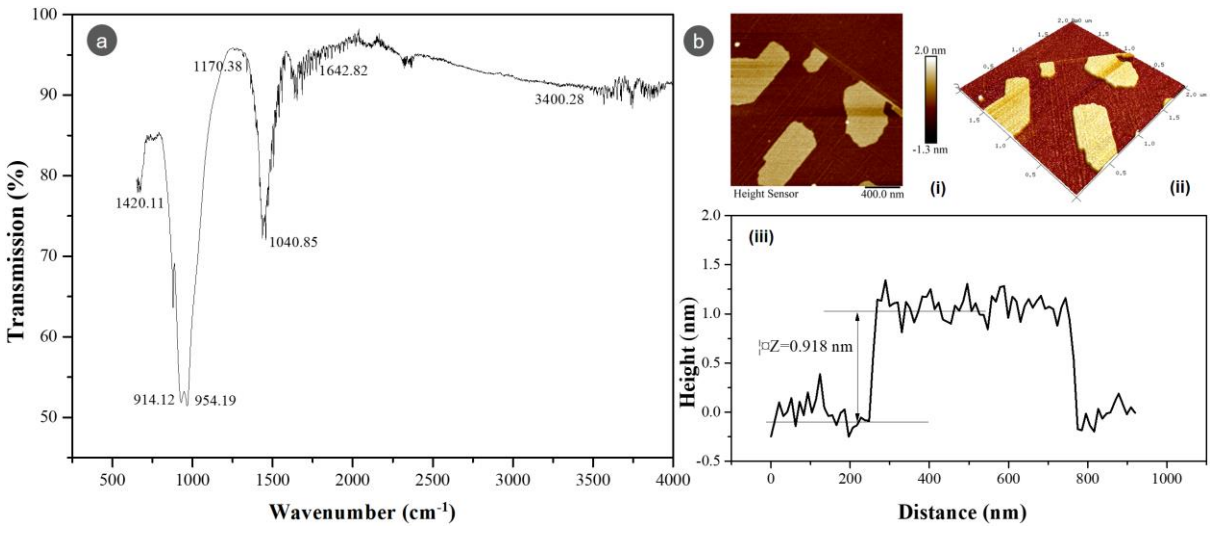

Fig. 5 Characterization of MaA by FTIR and AFM: (a) FTIR spectra, (b) Atomic force microscopy (AFM) imaging: (i) 2D Planar height surface, (ii) 3D surface morphology, (iii) Height-length contour with distance between 0 to 1000 nm.

3.2.4 DTG-DTA analysis

MaA is also distinguished and portrayed by DTG and DTA as shown in Fig. 6 and Table 1. It is noted from the DTA curve that there are two predominant peaks, which occur respectively after 100 and 300°C (Fig. 6a). The DTA curve also presents variable endothermic peaks.

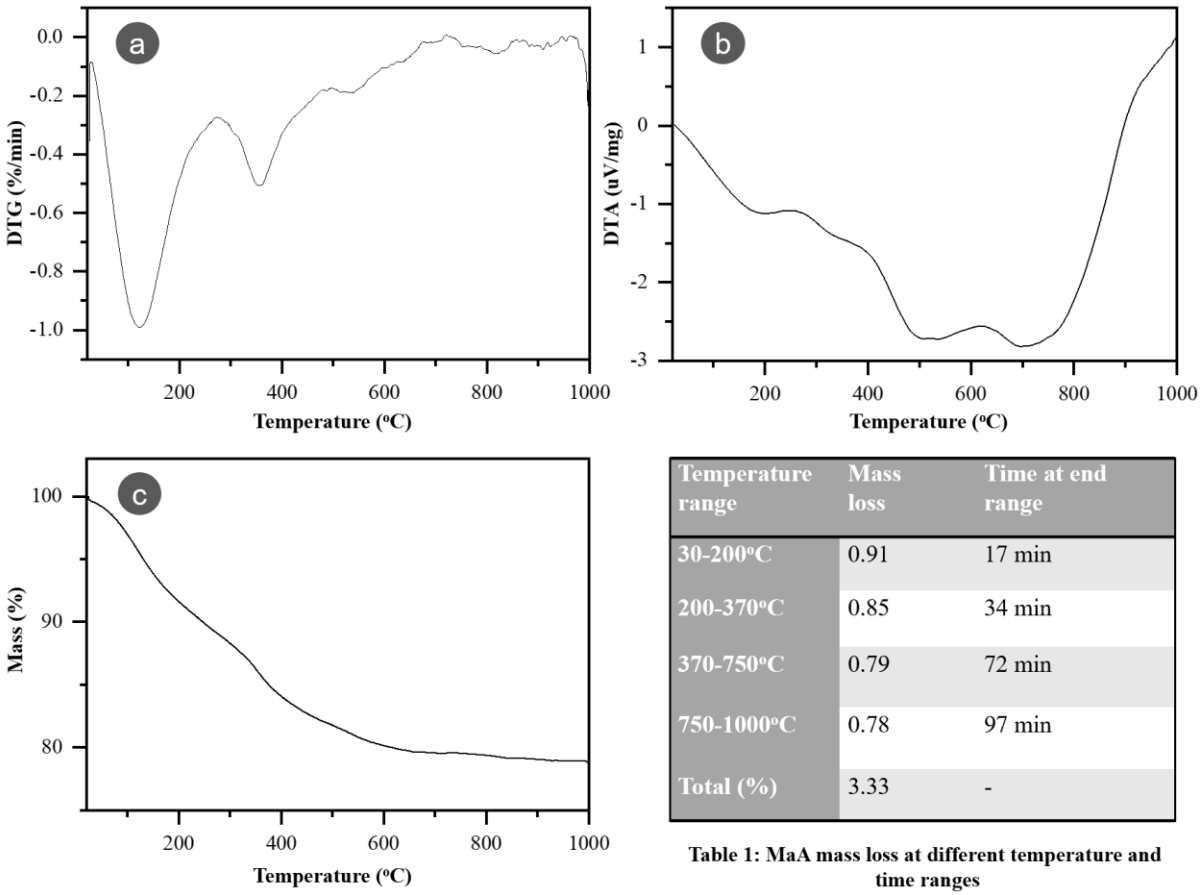

Temperature range	Mass loss	Time at end range
30-200°C	0.91	17 min
200-370°C	0.85	34 min
370-750°C	0.79	72 min
750-1000°C	0.78	97 min
Total (%)	3.33	-

Table 1: MaA mass loss at different temperature and time ranges

Fig. 6 DTG-DTA analysis of MaA: (a) Derivative thermogravimetry ratio, (b) Mass loss, (c) Differential thermal analysis, (Table 1) Mass loss with respect to the temperature and time ranges.

The endothermic peak occurring around 200°C in the DTA curve is abrupt and represents the removal of physically adsorbed water from the MaA configuration. Moreover, two consecutive endothermic crests are also noted at the broad thermal conditions from 500 to 800°C, indicating evaporation of the water tightly bound to the configuration as well as dehydroxylation by a greater water loss at higher temperatures (Fig. 6b). The curves describing the mass loss with regard to the temperature and their respective values are presented in Fig. 6c and Table 1. As shown, the mass loss is a function of the temperature increase. As a result, in the range of 30-1000°C, the mass loss drops from 0.91 to 0.78% with a total loss of 3.33%

317 within 97 min (Table 1), indicating that MaA is more porous and can be considered as an
318 adsorbent material.
319
320 *3.2.5 TEM electron microscope analysis*

321 To study the microscopic appearance and distribution of MaA adsorbent nanoparticles, the
322 TEM images are shown in Fig. 7. In general, the thinness of the fibers that make up MaA can
323 be clearly observed. The black specks below the fiber surface (Fig. 7a) are the result of the
324 aggregation and deposition of MaA nanoparticles at a later stage of synthesis. 2D pattern of a
325 SAED section was also captured (Fig. 7b). The pattern indicates diffraction spots, which are
326 related to the crystal structure of the sample. A large-scale single crystal was observed in the
327 structure by the aid of SEM and the image is displayed in Fig. 7c. As explained in section 3.2,
328 a moderate degree of nucleation is needed for the growth of large size crystal and a small
329 amount of nucleation can effectively supply enough reactive species in the reaction system.
330 The distinctive chemical elements are also evenly distributed on the surface of MaA, as
331 presented in Fig. 7 (d, e, f, g, h, i). O and Si are high-density elements with atomic fraction of
332 about 66.90% and 18.91%, respectively. Tiniest traces of Ca, Na, Mg and Al are also visible at
333 5.22%, 4.33%, 2.90% and 1.73% respectively. In light of the foregoing, it can be confirmed
334 with certainty that the synthetized MaA adsorbent is characterized by the discrete nanoparticles
335 with homogeneous pore surface, which results in the eminent adsorption property for the full
336 destruction of HM ions.

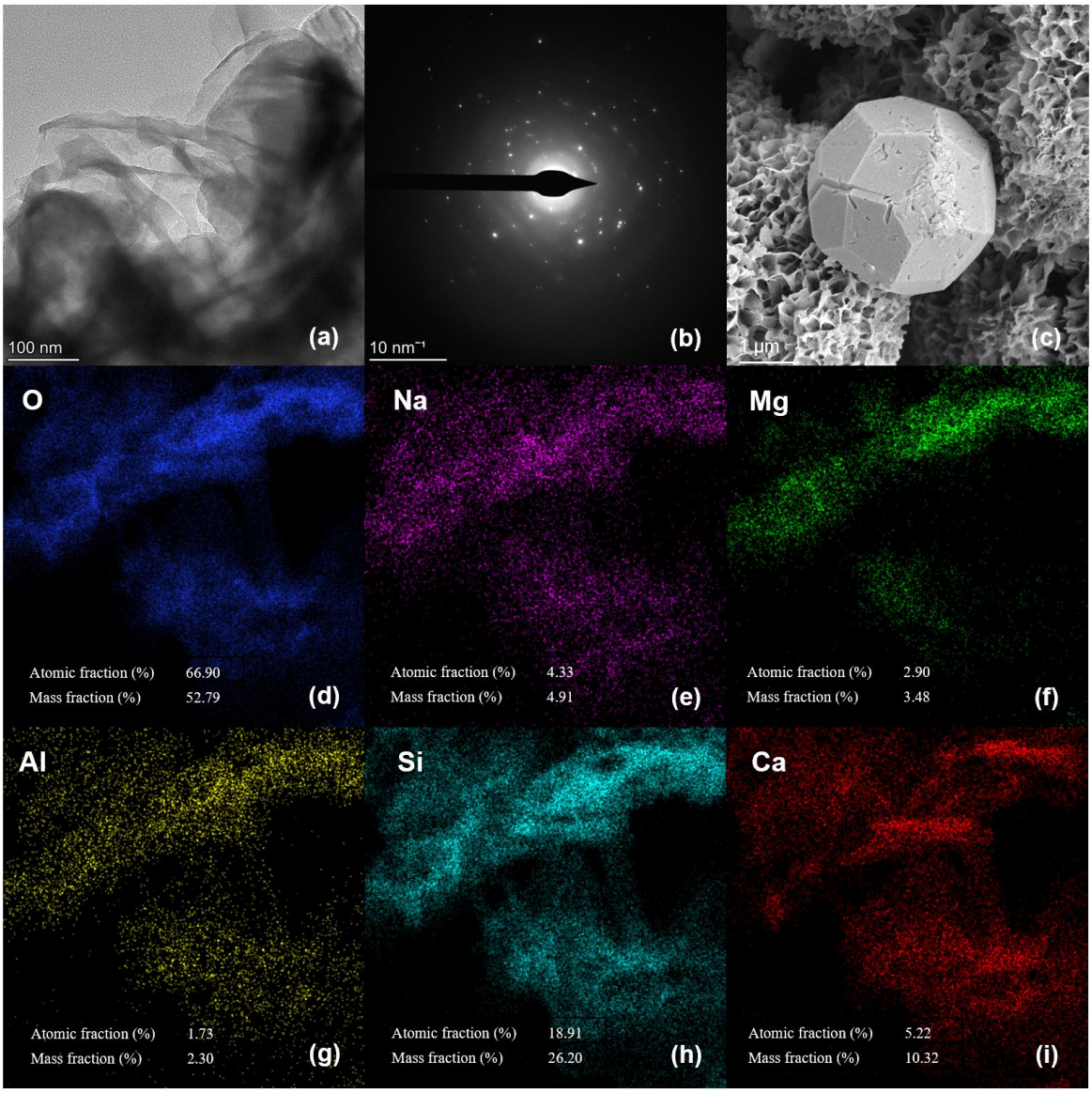

Fig. 7 TEM morphology of MaA: (a) TEM nanosheets imaging, (b) selected area electron diffraction (SAED) pattern, (c) SEM large scale single crystal of MaA, (d, e, f, g, h, i) Elemental mapping of O, Na, Mg, Al, Si and Ca at 100 nm scale.

3.3 Heavy metals adsorption capability of the MaA adsorbent

3.3.1 Effect of initial pH

The potential of hydrogen (pH) in solution influences the adsorbent by changing the exterior charge as well as the degree of protonation of the adsorbent, thus increasing the model ions in the solution. This aspect greatly influences the solution concentration and the adsorption process of heavy metals ions in wastewater [48, 49]. Because Pb^{2+}, Cd^{2+} and Cu^{2+} solutions

generate precipitation at different pH, this research only discusses the effect of adsorption of MaA at pH varying between 4~8. It is important to emphasize that these conditions can vary depending on the specific conditions of the solution, such as the presence of other ions and temperature. In this study, three different heavy metal solutions of Pb, Cd and Cu were prepared with initial concentration of 100 mg/L. A volume of 10 mL of the concentration was taken and mixed with 0.1 g of MaA. The slurry was then mixed separately in a thermostatic oscillator at the set conditions of temperature T=25℃, time t=1h and vibration frequency n=300 rpm/min. Afterwards, a volume of 10 mL of the homogeneous liquid of each metal was collected and adsorption experiment test was performed.

As shown in Fig. 8a, the adsorption rates of Pb^{2+}, Cd^{2+} and Cu^{2+} by MaA show different trends against pH level. The removal of Pb^{2+} by MaA at different pH presents rather linear trend compared to the other two metals. The removal rate rose with the increase of the pH of the adsorption mixture attaining the maximum of 95.83 mg/g at pH=8. However, it was also found from the same figure that, the removal of Cd^{2+} and Cu^{2+} by MaA has a higher adsorption rate at pH=6. A similar curve pattern was observed for both metals and the maximum removal rate was about 78.23 mg/g and 49.28 mg/g, respectively for Cd^{2+} and Cu^{2+}. Moreover, the elimination of Cu^{2+} was much lower than that of Pb^{2+} and Cd^{2+} at dissimilar pH values, and a net difference of the Cu solution color was observed after the addition of MaA (Fig. 8d). Notably, only the solution of Cu ion was evidently lighter blue and became transparent after the addition of MaA. The solution of Pb and Cd ions were colorless and transparent and retained their respective appearance even after addition of MaA adsorbent.

3.3.2 Effect of temperature

To better clarify the influence of thermal conditions on the removal of the studied metals by MaA, the pH value of the mixture was kept to 4.0-8.0, while temperature of the thermostatic oscillator was adjusted to 20℃, 25℃, 30℃, 35℃ and 40℃, respectively. The other conditions

were kept constant. The thermal impact on the adsorption efficiency is shown in Fig. 8b. Evidently, the adsorption of the heavy metals does not significantly increase when the temperature is ranged from 20-40℃. With further increase of the temperature to 25℃, the adsorption increases only slightly and is most remarkable in the Cu^{2+} ions solution. From these results, it can be concluded that the temperature does not have much influence on the elimination of the studied heavy metals. Consequently, ambient temperature (25°C) is recommended when MaA adsorbent is used for treating Pb^{2+}, Cd^{2+} and Cu^{2+} ions in wastewater. This novel combination can facilitate an ecologically friendlier, simpler and broader on-site application of MaA for the treatment of contaminated water.

3.3.3 Effect of contact time

The equilibration duration is of special significance while considering the economical aspect of wastewater reclamation and treatment. The transfer of metal ions induced by steering forces (vibration or concentration differential), the accessibility of active sites, etc. [50], and bonding interactions between metal ions and the adsorbent are some of the factors affecting equilibration duration. The impact of contact duration of MaA on the metals was also examined. The dosage of 0.1 mg/L of the adsorbent was adopted. Meanwhile, other parameters were regulated as follows: reaction temperature was 25 ℃, adsorption time was 0~1440 min, and the pH was 6. It was noticed that, at the first 60 min, the adsorption of Pb^{2+} and Cu^{2+} reached equilibrium, and Cd^{2+} approached equilibrium 2 h later, after a total contact time of 3h (Fig. 8c). The equilibrium adsorption amounts were 150.26 mg/g, 145.22 mg/g, and 148.19 mg/g, respectively for Pb^{2+}, Cd^{2+}, and Cu^{2+}. Moreover, the analysis indicated that the adsorbed amount of Pb^{2+} by MaA adsorbent was larger than that of the other two heavy metal ions, and the adsorption process in this case was faster than that of the other metals. In summation, a reaction period of 1h is needed for the adsorption to attain an equilibrium state when treating Pb and Cu ions, while 3h is needed for the total elimination of Cd metal ion. If all three metals

are treated simultaneously by MaA adsorbent, 3h treatment is recommended, which can simplify and suitably smooth the adsorption process.

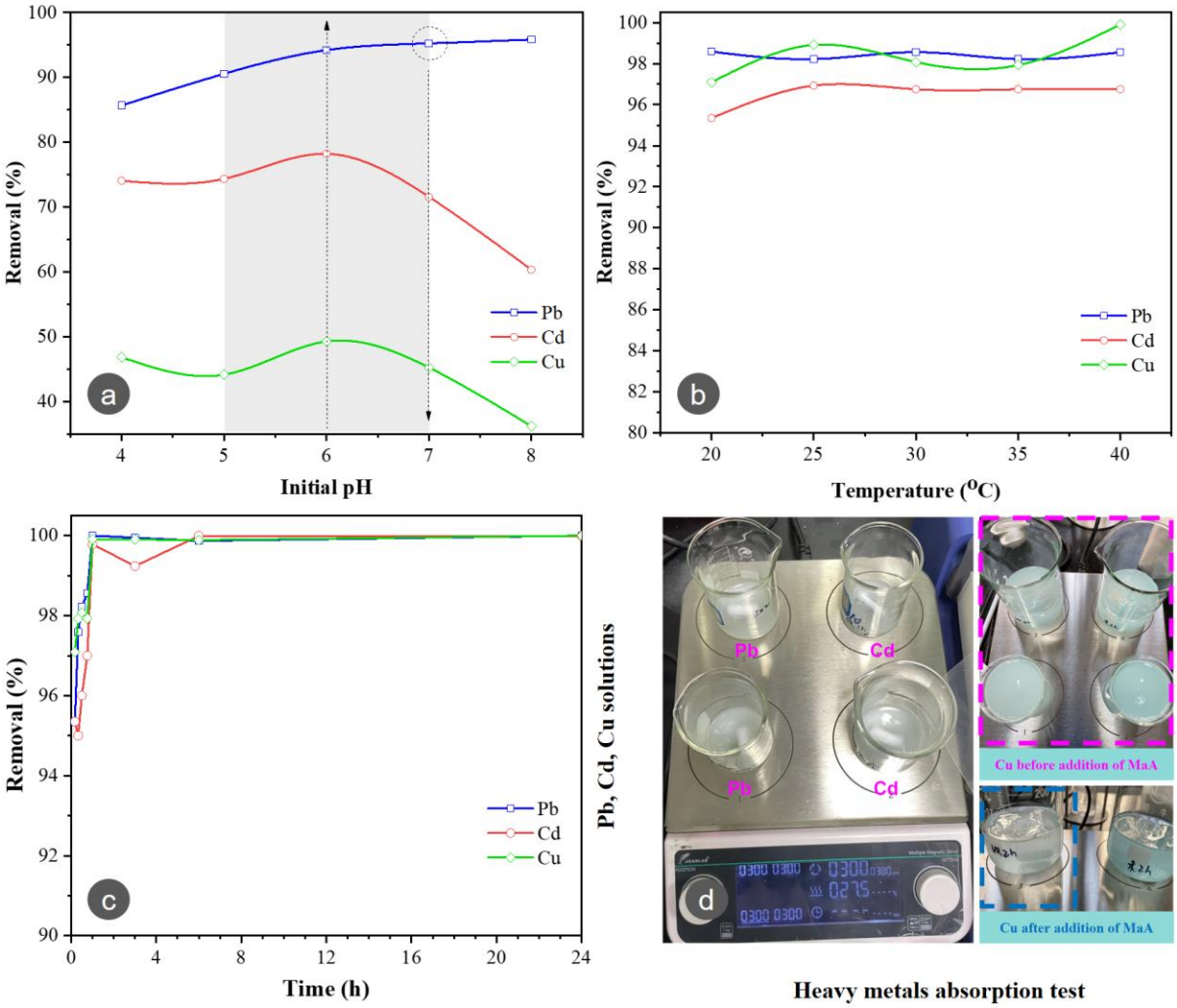

Fig. 8 Effect of different parameters on the heavy metals adsorption: (a) Initial pH, (b) Temperature, (c) Contact time, (d) Mixing of MaA into Pb, Cd, Cu solutions with thermostatic oscillator at the set conditions T=25°C, t=1h and n=300 rpm/min.

3.4 Adsorption isotherms of MaA adsorbent

The adsorption proficiency of the microporous MaA adsorbent was examined by analyzing its adsorption isotherms. Various models were employed to explain the experimental findings in the form of isothermic adsorption [51-53]. The Langmuir and Freundlich adsorption models were employed in this research to shed light into the final concentration and absorbed amount of the lead (Pb), cadmium (Cd) and copper (Cu) after addition of MaA adsorbent. The

Langmuir model describes monolayer adsorption, whereas the Freundlich model illustrates the process of heterogeneous adsorption. Langmuir model assumes that a monomolecular layer covers the surface of the adsorbent, and the adsorbates have the same force at the solid surface and do not interact with each other. It can be mathematically expressed by:

$$q_e = bq_m\rho_e/(1+\rho_e) \quad (3)$$

$$R_L = 1/(1+b\rho_0) \quad (4)$$

Where q_e denotes the equilibrium adsorption amount, b the Langmuir adsorption constant, q_m the saturated adsorption capacity. R_L designates the separation coefficient reflecting the magnitude of affinity between the adsorbent and adsorbate, $R_L>1$ (non-preferential adsorption), $R_L=1$ (linear adsorption), $0<R_L<1$ (preferential adsorption), $R_L=0$ (irreversible adsorption) [54, 55].

The Freundlich model, on the other hand, is a factual adsorption equation that predicts a non-homogeneous adsorption process with sites on the surface of the adsorbent having different adsorption energies, and is expressed as:

$$q_e = K_F\rho^{1/n} \quad (5)$$

Where K_F is the Freundlich constant, ρ denotes the adsorbate's equilibrium concentration and n is the Freundlich exponent [56, 57].

The kinetic adsorption models can also be used to express the speed of the adsorption during the process, with contact time as a variable. In this study, the adsorption kinetics of the studied heavy metals by MaA adsorbent was carried out by taking, respectively, 10 mL of Pb^{2+} Cd^{2+} and Cu^{2+} solution with a concentration of 100 mg/L. A mass m = 0.1 mg of MaA adsorbent was added into the solutions and the mixtures were subjected to a thermostatic oscillator under the conditions of 25°C, pH=6, n=300 rpm/min. The adsorption kinetics of the adsorbents are

mainly explored by two kinetic models, the quasi-primary kinetic model [58] and the quasi-secondary kinetic model [59]. The mathematical form of the model is:

$$ln(q_e - q_t) = ln\, q_e - \frac{k_1}{2.303} t \quad (6)$$

$$\frac{t}{q_t} = \frac{1}{k_2 q_e^2} \cdot \frac{t}{q_e} \quad (7)$$

Where t designates the adsorption time (min), q_t and q_e denote, respectively, the adsorption at time t, and the adsorbed amount per unit mass (mg/g) when equilibrium is reached. The quasi-primary kinetic rate constant (min^{-1}) is expressed through k_1 and the quasi-secondary kinetic rate constant [g/(mg min)] is expressed through k_2. Plotting t with the help of $lg(q_e-q_t)$ yields k_2. Plotting t with the help of t/q_t yields k_2 and q_e [60].

Table 1 Adsorption isotherm fitting by MaA

HM-id	Langmuir			Freundlich		
	$q_m/(mg \cdot g^{-1})$	$b/(L \cdot mg^{-1})$	R^2	K	$1/n$	R^2
Pb	75.0811	0.0323	0.9974	85.59	0.0418	0.1029
Cd	75.5300	0.1127	0.9956	114.4	0.2105	0.5858
Cu	74.0542	0.0701	0.9996	67.1	0.2471	0.5547

HM-id = Heavy metals identification

The process of adsorption of Pb, Cd and Cu on the MaA adsorbent were fitted using the contact time data in Fig. 7c, as shown in Table 1, where the correlation coefficients of Freundlich adsorption isotherm are R^2 = 0.1029, 0.5858, and 0.5547, respectively for Pb, Cd and Cu. Similarly, the R^2 of the respective metals are 0.9974, 0.9956, and 0.9996 for the Langmuir adsorption isotherm. The results indicate that the regression constant of the Langmuir isotherm is higher compared to the Freundlich isotherm. In addition, the adsorption data is in line with that of the Langmuir isotherm. In sum, the Langmuir adsorption isotherm equation can better characterize the adsorption process for the proper removal of Pb, Cd and Cu by using the microporous MaA adsorbent.

Table 2 Kinetic fitting by MaA

HM-id	$Q_{e,exp}/(mg \cdot g^{-1})$	Quasi-primary kinetic			Quasi-secondary kinetic		
		$Q_{e,cal}/(mg \cdot g^{-1})$	K_1/min^{-1}	R^2	$Q_{e,cal}/(mg \cdot g^{-1})$	$K_2/(g \cdot mg^{-1} \cdot min^{-1})$	R^2
Pb	1027	663.7	0.5412	0.2456	1074.3	0.00201	0.9933
Cd	306	163.2	0.5385	0.2341	323.6	0.00847	0.9991
Cu	239	100.8	0.5323	0.3084	249.3	0.01040	0.9971

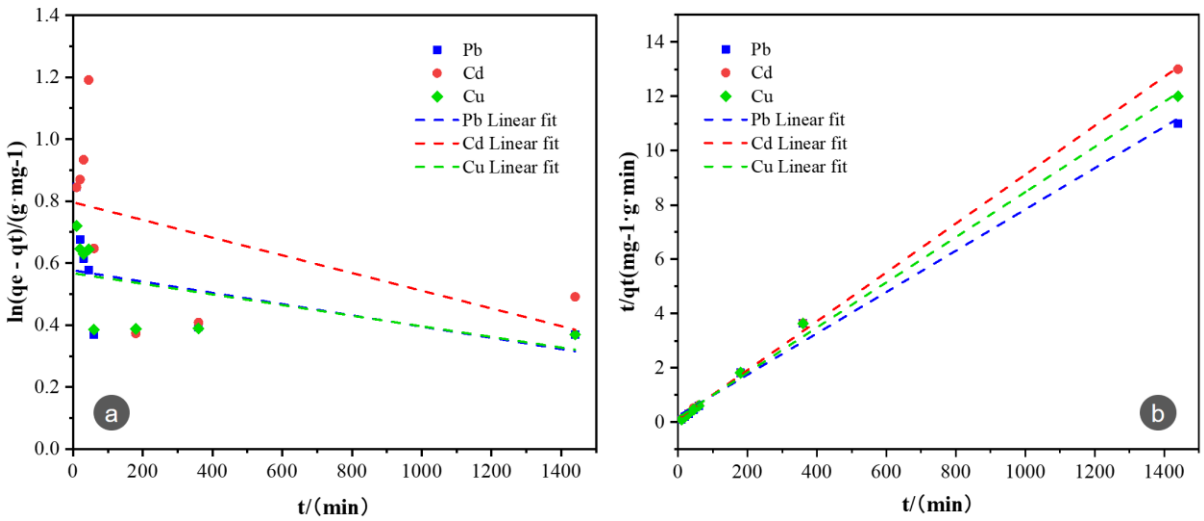

Fig. 9 Adsorption kinetics results: (a) Quasi-primary kinetic fitting, (b) Quasi-secondary kinetic fitting.

The results from the quasi-primary and quasi-secondary kinetic models are presented in Table 2 and Fig. 9. As shown, the coefficients of the quasi-primary kinetic models are estimated to R^2 = 0.2456, 0.2341, and 0.3084, respectively for Pb, Cd and Cu, whereas, for the quasi-secondary kinetic, the coefficients are 0.9933, 0.9991, and 0.9971. Accordingly, the results show that the quasi-secondary kinetic model presents the largest R^2 coefficient, good linear correlation, and the R^2 values obtained from all metals fitted better the kinetic equations compared to the values obtained for the quasi-primary reaction kinetic equations. The results denote that the general adsorption efficiency of Pb^{2+}, Cd^{2+} and Cu^{2+} by employing MaA is primarily controlled based on chemical process, deducible to the electron transfer or exchange by covalent forces between adsorbent and adsorbate. The adsorbent surface is charged during chemical adsorption, hence reacting with the metals. In addition, a conclusion can be drawn that, the adsorption of Pb^{2+}, Cd^{2+} and Cu^{2+} by MaA adsorbent prepared using waste glass is

more compatible with this model. Moreover, the obvious adsorption of all these heavy metals inherently occurs via the chemisorption mechanism, which plays a dominating role during the adsorption process [53, 61-63].

4. Conclusions

Waste glass-based microporous analcime adsorbent with high surface area was cogently synthesized through hydrothermal conditions. The optimum yield and permeability were achieved at a low thermal condition of 150^{o}C and NaOH molarity (3M). The adsorption capacity of the porous adsorbent was examined by removing lead (Pb), cadmium (Cd) and copper (Cu) from aqueous solution. It was intended as an efficient redress for contaminated water. This adsorbent eliminated, respectively, 150.26 mg/g and 148.19 mg/g of lead and copper after 1h of treatment and was able to absorb efficiently 145.22 mg/g of cadmium within 3 h. The obtained data are more consistent with the Langmuir adsorption model than the Freundlich adsorption model, suggesting that the process was a homogeneous monomolecular layer adsorption. Similarly, the adsorption kinetic results were congruent with the quasi-secondary kinetic equation, confirming that the process is mainly controlled by chemisorption process for expeditious elimination of Pb, Cd and Cu. In essence, this research proposes a simpler and cleaner procedure for producing pure and efficient adsorbent from waste glass powder, thus a new waste-to-useful resource. The experiments also demonstrated a harmless treatment of heavy metals that may be hazardous to human health.

■ Declaration of interests

The authors declare that they have no known competing financial interests or personal relationships that could have appeared to influence the work reported in this paper.

■ Acknowledgements

This work was supported by National Nature Science Foundation of China Grants No. 52108233. Acknowledgements are also given to Bi-carbon Special Program: Science and

Technology Special Program for Sustainable Development, Grant No. KCXST20221021111408021, and GJHZ20220913143007013; Shenzhen Science and Technology Program (Grant No. KCXFZ20230731093902006).

■ References

[1] Z. Hussain, Sultan, N., Ali, M., Naz, M. Y., AbdEl-Salam, N. M., & Ibrahim, K. A., Thermochemical Conversion of Waste Glass and Mollusk Shells into an Absorbent Material for Separation of Direct Blue 15 Azo Dye from Industrial Wastewater, ACS Omega (2020).

[2] Z.K. Hussain, A.; Sultan, N.; Ali, M.; Naz, M. Y.; Saed, K.; Sulaiman, S. A. , Thermo-chemical conversion of waste glass into non vitreous porous material for adsorption application, J. Mater. Cycles Waste Manage. 2019, 21, 1132−1143 (2019).

[3] C.M.R. Association, China Recycling Industry Development Report (2021), China Materials Recycling Association, Beijing, 2022.

[4] G. Crini, Lichtfouse, E., Wilson, L.D., and Morin, N., Conventional and non-conventional adsorbents for wastewater treatment, Environmental Chemistry Letters 17, pages195–213 (2019) (2019).

[5] M.S. Hosseini Hashemi, Eslami, F., and Karimzadeh, R., Organic contaminants removal from industrial wastewater by CTAB treated synthetic zeolite Y, Journal of Environmental Management 233, PP. 785–792 (2019).

[6] F.T. Fanta, Dubale, A.A., Bebizuh, D.F., and Atlabachew, M., Copper doped zeolite composite for antimicrobial activity and heavy metal removal from waste water, BMC Chemistry 13(1), PP 44 (2019).

[7] C. Söylemez, Türkmen, İ., and Özen, İ., Achieving Dual-Functionality by Surface Coating of Zeolite with Stearic Acid: Combining Breathability and Odor Control Properties in Polyethylene/Zeolite Composite Films, Macromolecular Research 28(12), PP.1149–1159 (2020).

[8] N. Keshavarzi, Mashayekhy Rad, F., Mace, A., Ansari, F., Akhtar, F., Nilsson, U., Berglund, L. and Bergström, L., Nanocellulose–zeolite composite films for odor elimination, ACS Applied Materials & Interfaces 7(26), PP.14254-14262 (2015).

[9] M.S.N. Lisbania V., Edwin E., Marta-Lena A., Farid A., Adsorption of heavy metals on natural zeolites: A review, Chemosphere 328 (2023).

[10] J. Darabdhara, Ahmaruzzaman, M., Recent developments in MOF and MOF based composite as potential adsorbents for removal of aqueous environmental contaminants, Chemosphere 304 (2022).

[11] S. Manikandan, Subbaiya, R., Saravanan, M., Ponraj, M., Selvam, M., Pugazhendhi, A., A critical review of advanced nanotechnology and hybrid membrane based water recycling, reuse, and wastewater treatment processes, Chemosphere 289 (2022).

[12] A.M. Awad, Shaikh, S.M.R., Jalab, R., Gulied, M.H., Nasser, M.S., Benamor, A., Adham, S., Adsorption of organic pollutants by natural and modified clays: a comprehensive review, Separ. Purif. Technol. 228, 115719 (2019).

[13] N.B. Singh, Nagpal, G., Agrawal, S., Rachna, Water purification by using adsorbents: a review, Environ. Technol. Innovat. 11, 187–240 (2018).

[14] C. Kaya, Ashraf, M., Alyemeni, M.N., Ahmad, P., Responses of nitric oxide and hydrogen sulfide in regulating oxidative defence system in wheat plants grown under cadmium stress, Physiol. Plantarum 168 (2019).

[15] C. Kaya, Okant, M., Ugurlar, F., Alyemeni, M.N., Ashraf, M., Ahmad, P., Melatonin-mediated nitric oxide improves tolerance to cadmium toxicity by reducing oxidative stress in wheat plants, Chemosphere 225, 627–638 (2019).

[16] S.K.V. M Samuel C., N. Vijayakumar, V Kanimozhi, S M. Arbaaz, R G S. Stacey, J Anusha, R. Choudhary, V. Lvov, G I. Tovar, F. Senatov, S. Koppala, S. Swamiappan,

548 Bioaccumulation of lead (Pb) and its effects on human: A review, Journal of Hazardous
549 Materials Advances 100094 (2022).
550 [17] J.A. Bhat, Ahmad, P., Corpas, F.J., Main nitric oxide (NO) hallmarks to relieve arsenic
551 stress in higher plants, J. Hazard Mater. 406 (2021).
552 [18] P. Ahmad, Alyemeni, M.N., Al-Huqail, A.A., Alqahtani, M.A., Wijaya, L., Ashraf, M.,
553 Kaya, C., Bajguz, A., Zinc oxide nanoparticles application alleviates arsenic (As) toxicity in
554 soybean plants by restricting the uptake of as and modulating key biochemical attributes,
555 antioxidant enzymes, ascorbate-glutathione cycle and glyoxalase system, Plants 9 (7), 1–18
556 (2020).
557 [19] X. Wang, Xu, J., Xu, M., Zhou, B., Liang, J., Zhou, L., High-efficient removal of arsenite
558 by coagulation with titanium xerogel coagulant, Separ. Purif. Technol. 258 (2021).
559 [20] X. Tang, Zheng, H., Teng, H., Sun, Y., Guo, J., Xie, W., Yang, Q., Chen, W., Chemical
560 coagulation process for the removal of heavy metals from water: a review, New Pub: Balaban
561 57 (4), 1733–1748 (2014).
562 [21] M.C. Benalia, Youcef, L., Bouaziz, M.G., Achour, S., Menasra, H., Removal of heavy
563 metals from industrial wastewater by chemical precipitation: mechanisms and sludge
564 characterization, Arabian J. Sci. Eng. 47 (5), 5587–5599 (2022).
565 [22] N.A.A. Qasem, Mohammed, R.H., Lawal, D.U., Removal of heavy metal ions from
566 wastewater: a comprehensive and critical review, Npj Clean Water 4 (1), 1–15 (2021).
567 [23] A. Dabrowski, Hubicki, Z., Podko´scielny, P., Robens, E., Selective removal of the heavy
568 metal ions from waters and industrial wastewaters by ion-exchange method, Chemosphere 56
569 (2), 91–106 (2004).
570 [24] U. Kamran, Rhee, K.Y., Lee, S.Y., Park, S.J., Innovative progress in graphene derivative-
571 based composite hybrid membranes for the removal of contaminants in wastewater: a review,
572 Chemosphere 306 (2022).

573 [25] A. Mohseni, Kube, M., Fan, L., Roddick, F.A., Treatment of wastewater reverse osmosis
574 concentrate using alginate-immobilised microalgae: integrated impact of solution conditions
575 on algal bead performance, Chemosphere 276, 130028 (2021).
576 [26] A. Azimi, Azari, A., Rezakazemi, M., Ansarpour, M., Removal of heavy metals from
577 industrial wastewaters: a review, Chem. Bio. Eng. Rev. 4 (1), 37–59 (2017).
578 [27] S. Mao, Gao, M., Functional organoclays for removal of heavy metal ions from water: a
579 review, J. Mol. Liq. 334 (2021).
580 [28] R. Shahrokhi-Shahraki, Benally, C., El-Din, M.G., Park, J., , High efficiency removal of
581 heavy metals using tire-derived activated carbon vs commercial activated carbon: insights into
582 the adsorption mechanisms, Chemosphere 264 (2021).
583 [29] N. Shao, Tang, S., Liu, Z., Li, L., Yan, F., Liu, F., Shun L., Zhang, Z. , Hierarchically
584 structured calcium silicate hydrate based nanocomposites derived from steel slag for highly
585 efficient heavy metal removal from waste water, ACS Sust. Chem. & Eng. 6, 14926−14935
586 (2018).
587 [30] A. Anderson, Anbarasu, A., Pasupuleti, R.R., Manigandan, S., Praveenkumar, T.R.,
588 Aravind Kumar, J., Treatment of heavy metals containing wastewater using biodegradable
589 adsorbents: a review of mechanism and future trends, Chemosphere 295 (2022).
590 [31] R. Chakraborty, Asthana, A., Singh, A.K., Jain, B., Susan, A.B.H., Adsorption of heavy
591 metal ions by various low-cost adsorbents: a review, Int. J. Environ. Anal. Chem. 102 (2), 342–
592 379 (2022).
593 [32] M.A. Barakat, New trends in removing heavy metals from industrial wastewater, Arab. J.
594 Chem. 4 (4), 361–377 (2011).
595 [33] Z.L. Yuxuan J. , Le H. , Yanbo Z. , Li L. , Siyu Z., Zhonghao P., Jiaxing L., Dongmin W.,
596 Synthesis of coal-analcime composite from coal gangue and its adsorption performance on
597 heavy metal ions,

598 Journal of Hazardous Materials 423 (2022) 127027 (2022).
599 [34] X. Wang, Wang, X., Pan, S., Yang, Q., Hou, S., Jiao, Y., Zhang, W., Occurrence of
600 analcime in the middle Jurassic coal from the Dongsheng Coalfield, northeastern Ordos Basin,
601 China, Int. J. Coal Geol. 196, 126–138 (2018).
602 [35] P. Iam-khong, Muchan, P., Sriprang, N., Nithitanakul, M., Synthesis and characterization
603 of a new phase of non Na-loaded analcime zeolite by microemulsion technique, Solid State Sci.
604 96, 105956 (2019).
605 [36] S.N. Azizi, Alavi Daghigh, A., Abrishamkar, M., Phase transformation of zeolite P to Y
606 and analcime zeolites due to changing the time and temperature, J. Spectrosc. 2013, 1–5 (2013).
607 [37] O.B. Kotova, Shabalin, I.N., Shushkov, D.A., Kocheva, L.S., Hydrothermal synthesis of
608 zeolites from coal fly ash, Adv. Appl. Ceram. 115, 152–157 (2016).
609 [38] S.N. Azizi, Daghigh, A.A., Abrishamkar, M., Synthesis of zeolites NaA and analcime
610 using rice husk ash as silica source without using organic template, J. Mater. Sci. 45, 5692–
611 5697 (2010).
612 [39] X. Ma, Yang, J., Ma, H., Liu, C., Zhang, P., Synthesis and characterization of analcime
613 using quartz syenite powder by alkali-hydrothermal treatment, Microporous Mesoporous
614 Mater. 201, 134–140 (2015).
615 [40] Y.-H. Hsiao, Ho, T.-Y., Shen, Y.-H., Ray, D., Synthesis of analcime from sericite and
616 pyrophyllite by microwave-assisted hydrothermal processes, Appl. Clay Sci. 143, 378–386
617 (2017).
618 [41] J.H. Taylor, Elmes, V.E., Hurt, A.P., Coleman, N.J., , Synthesis of feldspathoids and
619 zeolite K–F from waste amber container glass, Mater. Chem. Phys. 246, 122805 (2020).
620 [42] A.K. Varshneya, Fundamentals of Inorganic Glasses, second ed. , Academic Press Inc.,
621 San Diego, CA, 1994.

[43] Y. Ge, Tang, Q., Cui, X., He, Y., & Zhang, J. , Preparation of large-sized analcime single crystals using the Geopolymer-Gels-Conversion, Materials Letters 135, 15–18 (2014).

[44] L. Itani, Liu, Y., Zhang, W., Bozhilov, K. N., Delmotte, L., & Valtchev, V. , Investigation of the Physicochemical Changes Preceding Zeolite Nucleation in a Sodium-Rich Aluminosilicate Gel, Journal of the American Chemical Society 131(29), 10127–10139 (2009).

[45] S. Wang, Peng, X., Tang, L., Zeng, L., & Lan, C., Influence of inorganic admixtures on the 11Å-tobermorite formation prepared from steel slags: XRD and FTIR analysis, Construction and Building Materials 60, 42–47. (2014).

[46] P. Yu, Kirkpatrick, R. J., Poe, B., McMillan, P. F., & Cong, X., Structure of Calcium Silicate Hydrate (C-S-H): Near-, Mid-, and Far-Infrared Spectroscopy, Journal of the American Ceramic Society 82(3), 742–748. (2004).

[47] J. Bai, Li, Y., Xiang, J., Ren, L., Mao, M., Zeng, M., & Zhao, X., Preparation of the Monolith of Hierarchical Macro-/Mesoporous Calcium Silicate Ultrathin Nanosheets with Low Thermal Conductivity by Means of Ambient-Pressure Drying, Chemistry - An Asian Journal 10(6), 1394–1401. (2015).

[48] D.W. O'Connell, Birkinshaw, C., & O'Dwyer, T. F. , Heavy metal adsorbents prepared from the modification of cellulose: A review, Bioresource Technology 99(15), 6709–6724 (2008).

[49] M.N. El-Sayed, A. A. , Polyethylenimine − functionalized amorphous carbon fabricated from oil palm leaves as a novel adsorbent for Cr(VI) and Pb(II) from aqueous solution, J. Water Process Eng. 2017, 16, 296−308 (2017).

[50] S.Z.H. Mohammadi, H.; Moeinadini, Z., High surface area-activated carbon from Glycyrrhiza glabra residue by $ZnCl_2$ activation for removal of Pb(II)and Ni(II) from water samples, J. Ind. Eng. Chem. 20, 4112−4118. (2014).

[51] M.H.R. Givianrad, M.; Saber-Tehrani, M.; Aberoomand-Azar, P.; Sabzevari, M. H. , Preparation and characterization of nanocomposite, silica aerogel, activated carbon and its adsorption properties for Cd (II) ions from aqueous solution, J. Saudi Chem. Soc. 17, 329−335. (2013).

[52] S.O. Sornkamnerd, M. K.; Kaneko, T., Tough and porous hydrogels prepared by simple lyophilization of lC gels, ACS Omega 2017, 2, 5304−5314 (2017).

[53] Z.M.-S. Yousefi, A.; Tahmtan, R. A. M., Biosorption of chromium in aqueous solutions using Bivalve Mollusk Shells through central composite design (CCD) mode, Desalin. Water Treat. 2016, 57, 19877−19889 (2016).

[54] E. Wibowo, Rokhmat, M., Sutisna, Khairurrijal, & Abdullah, M., Reduction of seawater salinity by natural zeolite (Clinoptilolite): Adsorption isotherms, thermodynamics and kinetics, Desalination 409, 146–156 (2017).

[55] C.K. Lim, Bay, H. H., Neoh, C. H., Aris, A., Abdul Majid, Z., & Ibrahim, Z., Application of zeolite-activated carbon macrocomposite for the adsorption of Acid Orange 7: isotherm, kinetic and thermodynamic studies, Environmental Science and Pollution Research 20(10), 7243–7255 (2013).

[56] A. Nilchi, Saberi, R., Moradi, M., Azizpour, H., & Zarghami, R., Adsorption of cesium on copper hexacyanoferrate–PAN composite ion exchanger from aqueous solution, Chemical Engineering Journal 172(1), 572–580 (2011).

[57] W.S.W. Ngah, & Fatinathan, S., Adsorption characterization of Pb(II) and Cu(II) ions onto chitosan-tripolyphosphate beads: Kinetic, equilibrium and thermodynamic studies, Journal of Environmental Management 91(4), 958–969 (2010).

[58] Q. Qiu, Jiang, X., Lv, G., Chen, Z., Lu, S., Ni, M., J., Yan., Deng, X., Adsorption of heavy metal ions using zeolite materials of municipal solid waste incineration fly ash modified by microwave-assisted hydrothermal treatment, Powder Technology 335, 156–163 (2018).

671 [59] R. Ahmad, & Mirza, A., Adsorptive removal of heavy metals and anionic dye from
672 aqueous solution using novel Xanthan gum-Glutathione/Zeolite bionanocomposite,
673 Groundwater for Sustainable Development 7, 305–312 (2018).
674 [60] T.V. Gerasimova, Evdokimova (Galkina), O. L., Kraev, A. S., Ivanov, V. K., & Agafonov,
675 A. V. , Micro-mesoporous anatase TiO_2 nanorods with high specific surface area possessing
676 enhanced adsorption ability and photocatalytic activity, Microporous and Mesoporous
677 Materials 235, 185–194 (2016).
678 [61] A. Bouarioua, & Zerdaoui, M. , Photocatalytic activities of TiO 2 layers immobilized on
679 glass substrates by dip-coating technique toward the decolorization of methyl orange as a
680 model organic pollutant, Journal of Environmental Chemical Engineering 5(2), 1565–1574
681 (2017).
682 [62] B.H. Hameed, Ahmad, A. L., & Latiff, K. N. A. , Adsorption of basic dye (methylene blue)
683 onto activated carbon prepared from rattan sawdust, Dyes and Pigments 75(1), 143–149 (2007).
684 [63] M. Visa, Synthesis and characterization of new zeolite materials obtained from fly ash for
685 heavy metals removal in advanced wastewater treatment, Powder Technology 294, 338–347
686 (2016).

687